Metamagnetic transition and anomalous Hall effect in Mn-based kagomé magnets RMn_6Ge_6 (R=Tb-Lu)

Huibin Zhou,[1,2] Mengyi Shi,[3] Yuqing Huang,[1] Wenlong Ma,[1] Xitong Xu,[4] Junfeng Wang,[3] and Shuang Jia[1,5,6,*]

[1]*International Center for Quantum Materials, School of Physics, Peking University, Beijing 100871, China*

[2]*Spallation Neutron Source Science Center, Dongguan 523803, China*

[3]*Wuhan National High Magnetic Field Center and School of Physics, HuaZhong University of Science and Technology, Wuhan 430074, China*

[4]*Anhui Key Laboratory of Condensed Matter Physics at Extreme Conditions, High Magnetic Field Laboratory, HFIPS, Anhui, Chinese Academy of Sciences, Hefei 230031, China*

[5]*Interdisciplinary Institute of Light-Element Quantum Materials and Research Center for Light-Element Advanced Materials, Peking University, Beijing 100871, China*

[6]*CAS Center for Excellence in Topological Quantum Computation, University of Chinese Academy of Sciences, Beijing 100190, China*

(Received 15 September 2021; revised 8 December 2022; accepted 25 January 2023; published 13 February 2023)

We investigate electrical transport and magnetic properties of the single-crystalline, Mn-based kagomé magnets RMn_6Ge_6 (R=Tb-Lu). The compounds mostly feature a series of magnetic orderings of R and Mn moments at different temperatures and metamagnetic transition (MMT) under an external magnetic field. We classify the MMT into three types, i.e., from skewed spiral to a structure containing decoupled R and Mn moments, from antiferromagnetic to flat spiral Mn moments, and from flat spiral to a ferrimagnetic state of R and Mn moments. The former two induce a small anomalous Hall effect (AHE), whereas the latter gives rise to a large one. We conclude that ferromagnetic ordered Mn moments in the kagomé lattice lead to a significant AHE, while other magnetic structures of R and Mn moments do not. The AHE in $TbMn_6Ge_6$ generally has an intrinsic origin, while no clear sign of intrinsic AHE is found in other compounds.

DOI: 10.1103/PhysRevMaterials.7.024404

I. INTRODUCTION

Transition-metal-based, intermetallic kagomé magnets have attracted great attention due to their exotic quantum physics induced by interplay among the crystal structure, magnetism, and topological properties [1–9]. A kagomé lattice, consisting of a two-dimensional network of corner-sharing triangles, naturally hosts both relativistic and dispersionless electrons, which are the origins of its Dirac-type band crossing and flat band. Exotic quantum phases emerge in a kagomé lattice with the inclusion of magnetism and spin-orbit coupling. One example is a long-sought, Chern-gapped, massive Dirac fermion (MDF) which can give rise to a high-temperature quantum anomalous Hall effect [9–11]. Recently, the MDF was discovered in a defect-free, strong out-of-plane ferromagnetic (FM) Mn kagomé lattice in the Chern topological magnet $TbMn_6Sn_6$ [12]. Topological transverse thermoelectric effects associated with the Berry curvature from the massive Dirac gaps have also been observed in this quantum magnet [13,14]. Further studies on the members of RMn_6Sn_6 (R=rare earth elements) demonstrated that magnetic textures are closely related to the quantum phenomena in the Mn kagomé lattice [15–19]. When the rare earth elements are Sc, Y, and Lu with a nonmagnetic moment, the compounds show a flat spiral (FS) configuration of the Mn moments as the ground state in zero external field [20–22]. When R bears a $4f$ local moment, the magnetic interaction between the Mn and R moments varies, leading to a FM state for R=Nd and Sm [23], a ferrimagnetic (FIM) state for R=Gd to Ho, and an antiferromagnetic (AFM) state for R=Er and Tm [24,25]. The RMn_6Sn_6 compounds with novel magnetic textures may host nontrivial topological phases, geometric frustration, and a flat electronic band [20,21,26] and have potential applications in microscale quantum devices [27]. Investigation of the anomalous Hall effect (AHE) in the RMn_6Sn_6 series unveiled that the R atoms can effectively drive the Chern gap and chemical potential of the MDF hosted in the Mn kagomé lattice in FIM RMn_6Sn_6 [15]. Beyond rare earth elements, the kagomé ferromagnet $LiMn_6Sn_6$ also exhibits a large intrinsic AHE [28]. It can be seen that this versatile magnetic family has the potential to be a model system for studying topological electrons hosted in the kagomé lattice. However, the complex magnetic structures in this family have led to obstacles to the in-depth study of their novel quantum phenomena.

In order to gain insight into the magnetic structures, magnetic phase transitions, and their induced AHE in Mn-based kagomé magnets, we focus on the magnetic and electrical transport properties of a family of isostructural RMn_6Ge_6 (R=Tb-Lu) compounds. RMn_6Ge_6 consists of segregated manganese atom kagomé layers [Fig. 1(a)], similar to RMn_6Sn_6. Previous magnetization and neutron diffraction studies demonstrated that the members of RMn_6Ge_6 exhibit a wide variety of magnetic structures and a wealth of phase transitions, more complex than those in RMn_6Sn_6 [29–37]; therefore, the RMn_6Ge_6 compounds could serve as an

*gwljiashuang@pku.edu.cn

 ©2023 American Physical Society

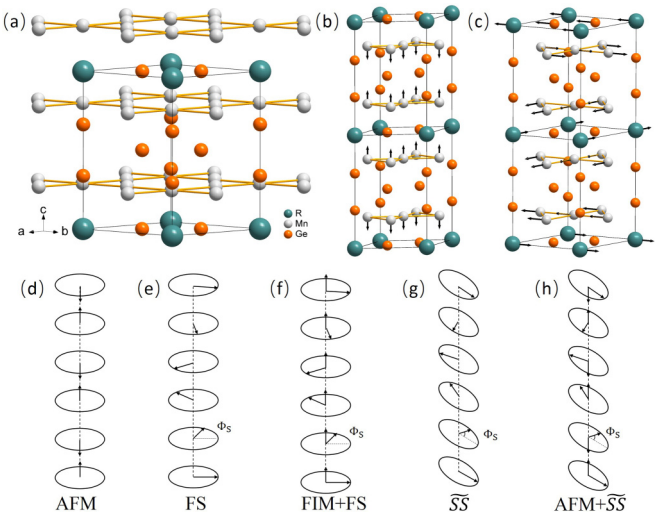

FIG. 1. Crystal and magnetic structures of RMn$_6$Ge$_6$. (a) Crystal structure of RMn$_6$Ge$_6$ showing layered stacking along the c axis. (b) and (c) Schematic representations of the moment arrangement of antiferromagnetic (AFM) and flat spiral (FS) structures in RMn$_6$Ge$_6$, respectively. (d)–(h) Intuitive model representations of the AFM, FS, ferrimagnetic flat spiral (FIM+FS), skewed spiral ($\widetilde{SS}$), and antiferromagnetic skewed spiral (AFM+$\widetilde{SS}$) magnetic structures, respectively. The schemes are based on the results of Refs. [29–35].

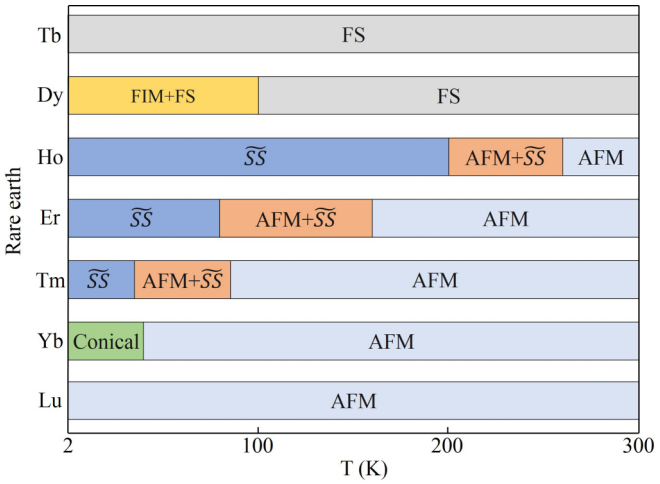

FIG. 2. Schematic magnetic phase diagram of RMn$_6$Ge$_6$ in zero field as a function of temperature obtained from the results of neutron diffraction [29–35].

interesting playground for studying the relationship between the magnetic structures and the related AHE. In general, the RMn$_6$Ge$_6$ compounds exhibit higher magnetic ordering temperatures than RMn$_6$Sn$_6$ [38]. For nonmagnetic R compounds, LuMn$_6$Ge$_6$ shows an up-up-down-down collinear AFM ordering of Mn moments [Fig. 1(b)] [35,39], unlike LuMn$_6$Sn$_6$, which exhibits an FS magnetic structure of Mn moments [40]. For R = Y, Zr, and Hf, the magnetic arrangement evolves to a double-cone AFM structure at low temperature [39–41]. For 4f-moment-bearing RMn$_6$Ge$_6$, the 4f moments of the heavy rare earth tend to develop an antiparallel configuration to the Mn moments, while the strength of the magnetic coupling varies for different R atoms and temperatures [42]. Competition between the Mn-Mn, R-Mn, and R-R interactions leads to various magnetic structures when temperature changes. For TbMn$_6$Ge$_6$ and DyMn$_6$Ge$_6$, which have relatively strong R-Mn magnetic interaction, the structure is characterized by an FS configuration which is constructed by two layers of Mn and one layer of R moments confined in the basal plane [Fig. 1(c)]. The moment direction spirals collectively along the c axis to form the FS structure [Fig. 1(e)] [29,30,43]. On the other hand, because the members with R=Ho, Er, Tm, and Yb have relatively weak R-Mn coupling, their room-temperature magnetic structure is characterized by an AFM-ordering Mn sublattice and nonordering R moments. At lower temperature, the magnetic ordering of Mn moments renders a transition from an AFM to a helimagnetic skewed spiral ($\widetilde{SS}$) structure. Complicated magnetic structures were observed in the RMn$_6$Ge$_6$ compounds at intermediate temperature, like the FIM flat spiral [FIM+FS; Fig. 1(f)] and AFM skewed spiral [AFM+$\widetilde{SS}$; Fig. 1(h)]. According to the experimental results for powder neutron diffraction [29–35], we summarize the magnetic structures of the family of RMn$_6$Ge$_6$ (R=Tb-Lu) at zero external field from 300 to 2 K as shown in Fig. 2.

Roughly understanding the magnetic structures of RMn$_6$Ge$_6$, we infer that a spontaneous AHE is absent because no FM and FIM states were observed. On the other hand, because the RMn$_6$Ge$_6$ and RMn$_6$Sn$_6$ families have the same crystal structure highlighted by the Mn-based kagomé lattice, it is interesting to investigate whether RMn$_6$Ge$_6$ hosts similar topological electronic structures. Before doing any detailed band structure calculations and electron spectral measurements, we believe a survey of the AHE for RMn$_6$Ge$_6$ under magnetic field at various temperatures will be instructive because the intrinsic AHE is a hallmark of nontrivial topology. Understanding the relationship between different types of metamagnetic transitions (MMTs) and AHEs may help us to unveil how the magnetic structure change affects potential topological electrons hosted in the kagomé lattice. Unfortunately, the electrical transport property of single-crystalline samples has not been reported [44], as far as we are aware. In this paper we present a systematic study of the MMTs and AHEs in RMn$_6$Ge$_6$ (R=Tb-Lu) and find that they generally exhibit an MMT-related AHE in an external magnetic field. We observed a significant intrinsic AHE as long as the Mn kagomé lattice shows an FM configuration when the magnetic structure changes from FS to FIM. In comparison, the AHE caused by other magnetic structures of R and Mn moments is much weaker. This observation demonstrates that the Mn-based kagomé lattice is crucial for the AHE, while the role of R magnetism in the AHE of the "166" family is through the R-Mn interactions. There may be a considerable intrinsic AHE in TbMn$_6$Ge$_6$, while no obvious feature of an intrinsic AHE was observed in other materials except the Tb compound.

This paper is organized as follows. Section II gives the experimental method. The magnetic and electrical transport properties for the RMn$_6$Ge$_6$ family are given in Sec. III. To make the writing organized, we divide the results section into three subsections. In Sec. III A, we give the results for

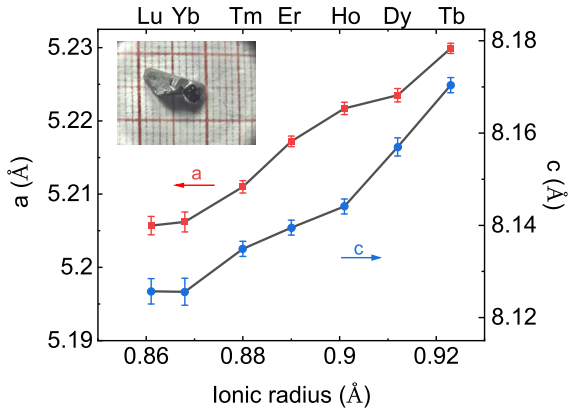

FIG. 3. Lattice parameters a and c for $R\mathrm{Mn_6Ge_6}$ (R=Tb-Lu) versus the radius of R^{3+} ions with a coordination number equal to 6 [46]. The inset shows a photo of the $\mathrm{LuMn_6Ge_6}$ single crystal.

$\mathrm{TbMn_6Ge_6}$ and $\mathrm{DyMn_6Ge_6}$, both of which exhibit the FS-type magnetic structure in a large temperature range in zero field. In Sec. III B, we focus on the AHE induced by other types of MMTs in $R\mathrm{Mn_6Ge_6}$ (R=Ho-Yb). In Sec. III C, we show the AHE in $\mathrm{LuMn_6Ge_6}$, which has no $4f$ moment. We discuss the mechanism and scaling of the AHE for $\mathrm{TbMn_6Ge_6}$ in Sec. IV. Section V presents our conclusions.

II. METHOD

Single crystals of $R\mathrm{Mn_6Ge_6}$ (R=Tb-Lu) were synthesized using a Ge self-flux method. Unlike previous studies which choose Ga and In as the flux [38], the Ge flux avoids the introduction of a fourth element which can be a substitution on the Ge site. The details of the crystal growth can be found in the Supplemental Material [45]. The crystal structure was examined with powder x-ray diffraction measurements using a Rigaku Mini-flux 600 diffractometer with Cu $K\alpha$ radiation. Figure 3 shows that lattice parameters a and c for $R\mathrm{Mn_6Ge_6}$ (R=Tb-Lu) compounds, obtained using the RIETICA Rietveld refinement program, approximately follow the lanthanide contraction, with no exception for $\mathrm{YbMn_6Ge_6}$. This result is consistent with the report in the literature [38].

Magnetization and electrical transport measurements were carried out using a Quantum Design magnetic property measurement system (MPMS) and physical property measurement system, respectively. Resistivity and Hall resistivity measurements were performed using a standard four-probe method on single crystals cut into a rectangular shape. For Hall measurements in the ab plane, a field was applied along the c axis with current and voltage in the ab plane. For Hall measurements perpendicular to the ab plane, a magnetic field and current were applied orthogonally in the ab plane, and an out-of-plane voltage was measured. The Hall resistivity was extracted from total Hall signals with $\rho_{yx}(\mu_0 H) = [\rho(+\mu_0 H) - \rho(-\mu_0 H)]/2$ to get rid of the resistivity contribution due to voltage probe misalignment.

III. EXPERIMENTAL RESULTS

A. $\mathrm{TbMn_6Ge_6}$ and $\mathrm{DyMn_6Ge_6}$

Magnetic and electrical transport properties for $\mathrm{TbMn_6Ge_6}$ and $\mathrm{DyMn_6Ge_6}$ are presented together because they manifest

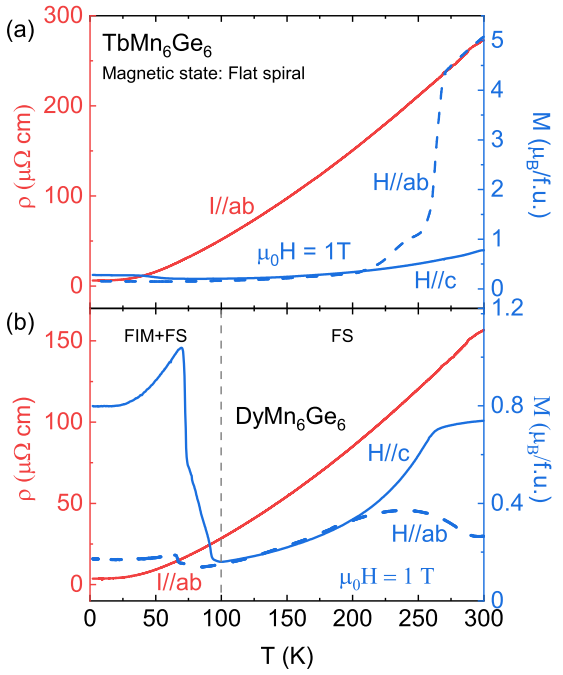

FIG. 4. Magnetization and resistivity as a function of temperature for (a) $\mathrm{TbMn_6Ge_6}$ and (b) $\mathrm{DyMn_6Ge_6}$.

the same FS magnetic structure below room temperature. The FS structure is a ground state for $\mathrm{TbMn_6Ge_6}$ in zero field in the whole temperature range [29], while a c-direction FIM state is superimposed on the FS structure for $\mathrm{DyMn_6Ge_6}$ below 100 K.

Figure 4 shows the temperature dependence of magnetization M for $\mathrm{TbMn_6Ge_6}$ and $\mathrm{DyMn_6Ge_6}$ when an external magnetic field $\mu_0 H = 1$ T is applied along the crystallographic c axis and in the ab plane. $M(T)$ for $\mathrm{TbMn_6Ge_6}$ is nearly invariant when $H \parallel c$, while $M(T)$ for $H \parallel ab$ is largely enhanced above 200 K. A previous study showed that the increase in M from 200 to 450 K is due to a small critical field of the FS structure [47]. We do not observe any spontaneous magnetization in the single crystal, unlike in Ref. [48].

The $M(T)$ profile of $\mathrm{DyMn_6Ge_6}$ for $H \parallel c$ features a gradual decrease with decreasing temperature above 100 K and then a sudden increase at this temperature, similar to what was observed in Ref. [38]. This feature is consistent with the neutron scattering experiment which suggested that $\mathrm{DyMn_6Ge_6}$ has an FS magnetic structure of Dy and Mn moments below 360 K and then further develops a small out-of-plane FIM component below 100 K [30]. The $M(T)$ curve with $H \parallel ab$ shows a manner opposite to that with $H \parallel c$ between 250 and 300 K, indicating that the easy direction changes. The $\rho(T)$ curves for $\mathrm{TbMn_6Ge_6}$ and $\mathrm{DyMn_6Ge_6}$ show no anomaly below room temperature.

To elucidate the relationship between the Hall effect and magnetic structure change, we systematically examine the $M(H)$ curves and corresponding Hall signals. Figure 5 exhibits the field dependence of M and ρ_{yx} for $\mathrm{TbMn_6Ge_6}$ at several representative temperatures when an external field is along the c axis and in the ab plane. These isotherms display very different shapes, depending on the temperatures

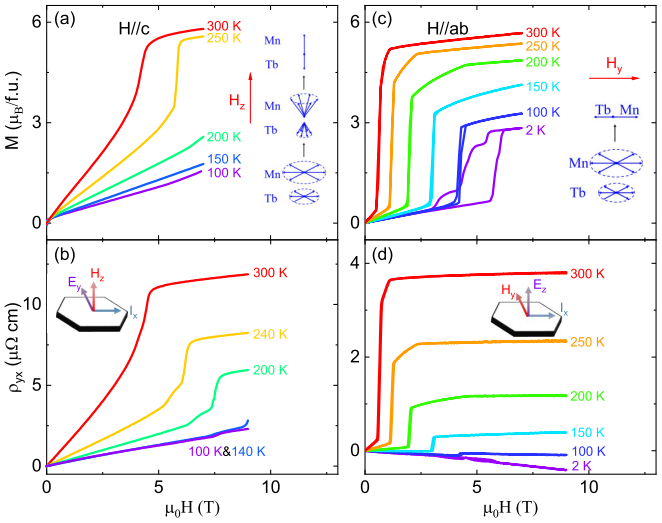

FIG. 5. Magnetization and Hall resistivity as a function of magnetic field $\mu_0 H$ for $TbMn_6Ge_6$ single crystals at several representative temperatures when $H \parallel c$ and $H \parallel ab$ plane. Insets in (a) and (c) indicate changes in the moment configurations as the magnetic field increases. The measurement configurations for ρ_{yx} and ρ_{zx} are shown in the insets of (b) and (d), respectively.

and magnetic field directions. The curves for $H \parallel c$ show a saturating plateau at relatively high temperature and magnetic field, while in the curves for the $H \parallel ab$ plane the saturation occurs at much lower field. This observation indicates that $TbMn_6Ge_6$ is an easy-plane system, in good agreement with the FS structure obtained from the neutron diffraction experiment [29]. Below 100 K, the $M(H)$ curves show strong hysteretic behavior for the $H \parallel ab$ plane.

The magnetic moment arrangements that account for the transitions are shown in the insets in Figs. 5(a) and 5(c). The moments in the FS structure are gradually bent out of the basal plane to form a double-cone structure in an external field along the c axis and then finally to form an FIM configuration in which the Tb moment is antiparallel to the Mn moments. When $H \parallel ab$ plane, the FS structure directly changes to an FIM ordering in the plane formed by an antiparallel, FM ordered Tb and Mn sublattice.

Figures 5(b) and 5(d) show that the $\rho_{yx}(H)$ curves roughly resemble the profile of $M(H)$. After the transition occurs, $\rho_{yx}(H)$ shows a large saturated anomalous term for both $H \parallel c$ axis and $H \parallel ab$ plane. This anomalous contribution can be traced to low temperature, although the magnitude is significantly suppressed because of the small ρ.

It is noteworthy that $\rho_{zx}(H)$ shows a negative dependence on H at low temperatures, which is opposite to any other Hall resistivity $\rho_{yx}(H)$ for RMn_6Ge_6. Obviously, it comes from the negative normal Hall coefficient, and we analyze the data in the Sec. IV.

$M(H)$ and ρ_{yx} curves for $DyMn_6Ge_6$ at several representative temperatures recorded for $H \parallel c$ axis are displayed in Fig. 6. A complicated magnetization process was reported in Refs. [22,38], and our results are consistent. From 2 to 50 K we observe a small zero-field spontaneous magnetization (about 0.5 μ_B/f.u. at 2 K), which is the result of a small FIM component reported in the neutron scattering experiment [30].

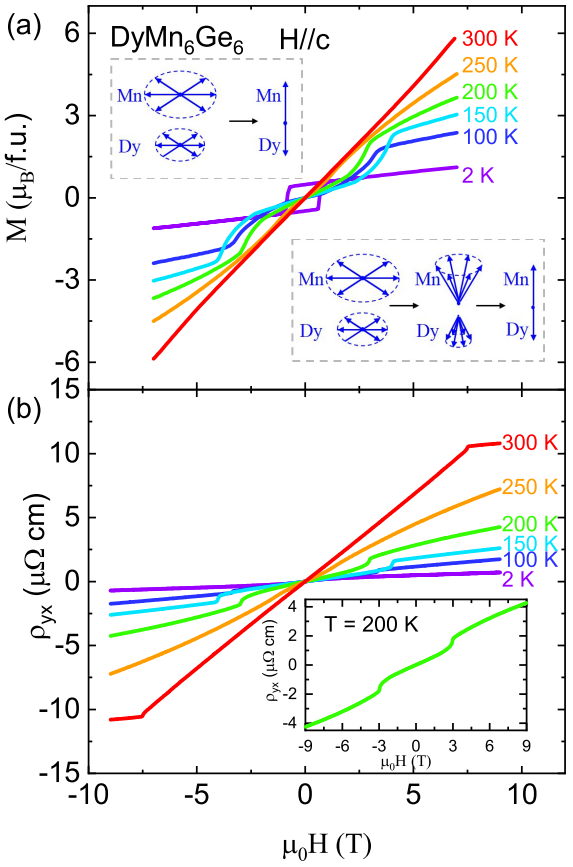

FIG. 6. Field dependence of (a) magnetization and (b) Hall resistivity for the $DyMn_6Ge_6$ single crystal at several representative temperatures when $H \parallel c$. Bottom right and top left insets in (a) display the evolutions of the FS structure at intermediate and high temperatures when the applied field increases, respectively. The inset in (b) shows the field dependence of ρ_{yx} at 200 K.

From 60 to 240 K there is a weak transition at low field, above which the magnetization gradually increases with the field. Above 240 K the transition fades out, and the magnetization gradually increases up to 7 T, which is the highest field we applied in magnetization measurements. The MMT of the FS state at intermediate temperatures is the same as those in $TbMn_6Ge_6$ [see the inset in Fig. 6(a)].

Checking the ρ_{yx} curves, we find no spontaneous AHE at low temperatures. Between 100 and 250 K, the ρ_{yx} curves show a small jump due to the formation of a double-cone structure [see the individual curve at 200 K in the bottom right inset in Fig. 6(b)]. Near 300 K we see a linear field-dependent ρ_{yx} up to 7.5 T, above which ρ_{yx} is saturated at the FIM state, leading to large anomalous Hall resistivity.

B. RMn_6Ge_6 (R=Ho-Yb)

The temperature dependences of the electrical resistivity and magnetization for RMn_6Ge_6 (R=Ho-Yb) have different characteristics than those for their Tb and Dy siblings (Fig. 7). As the temperature decreases from 300 K, $M(T)$ curves gradually increase, and then they feature a cusp at around 215, 110, 60, and 50 K for R=Ho, Er, Tm, and Yb, respectively, following a complicated dependence at lower temperature. For $HoMn_6Ge_6$, a pronounced increase in the magnetization

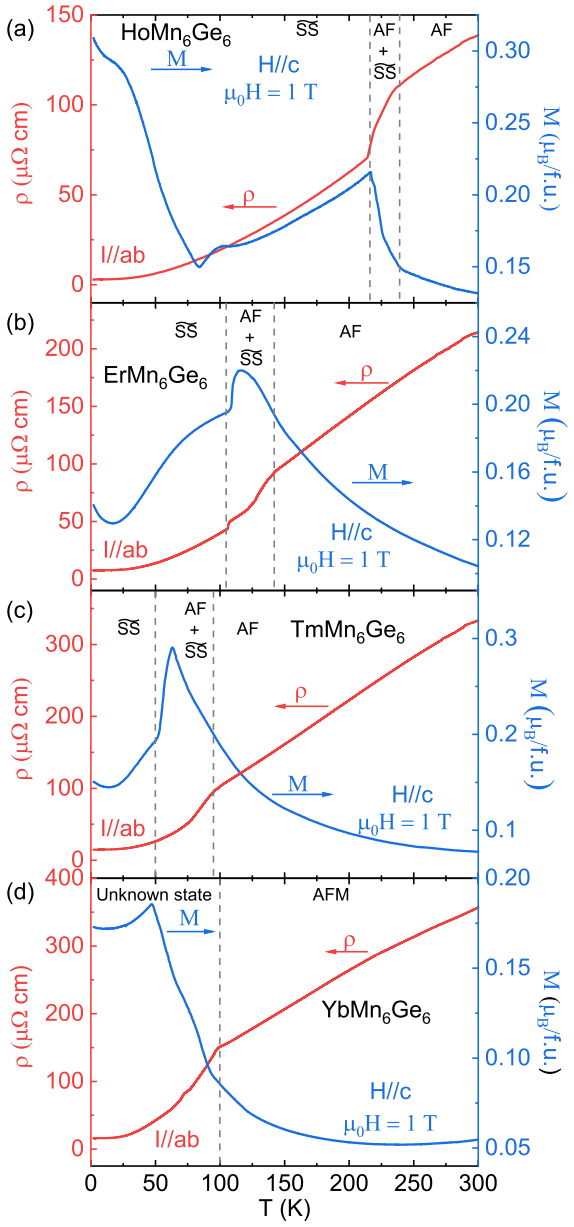

FIG. 7. Temperature dependence of resistivity and magnetization for (a) $HoMn_6Ge_6$, (b) $ErMn_6Ge_6$, (c) $TmMn_6Ge_6$, and (d) $YbMn_6Ge_6$.

occurs below 80 K. This feature was also observed in polycrystalline samples and was attributed to the enhancement of the Ho moment at low temperature [31].

Correspondingly, $\rho(T)$ curves show sharp knee points near the cusp temperature on the $M(T)$ curves [44,49]. Previous studies unveiled that the magnetic structures for R=Ho, Er, and Tm evolve from an AFM arrangement of Mn moments and no ordering of R moments at room temperature to a superposition of an $\widetilde{SS}$ structure of the R moment with an AFM component of the Mn sublattice at intermediate temperature [31–33]. At low temperature, the R and Mn moments order in an $\widetilde{SS}$ structure which does (for Ho) or does not (for Er and Tm) undergo easy direction changes at the base temperature. We label the boundaries of three magnetic ordering regions ($\widetilde{SS}$, AFM+$\widetilde{SS}$, and AFM) in Fig. 7. Here the magnetic ordering of R moments develops at much lower temperature than the Mn moment, but it seems to largely affect the electron scattering because the $\rho(T)$ curves show a significant slope change when the magnetic structure changes.

Magnetic ordering of $YbMn_6Ge_6$ seems to be slightly different from that for the other three. While the cusp on the $M(T)$ curve occurs at about 50 K, the $\rho(T)$ curve changes slope at around 100 K, which may indicate a hidden magnetic transition that was not reported before. Magnetic structures of $YbMn_6Ge_6$ have not been fully identified yet [34].

We now check the magnetization and Hall resistivity as a function of magnetic field at different temperatures (Fig. 8). At first glance, their $M(H)$ isothermals are, in general, less in magnitude than those for $TbMn_6Ge_6$ and $DyMn_6Ge_6$. An MMT generally occurs at the $M(H)$ isothermal at room temperature for all four compounds. This transition moves to higher field, which exceeds 9 T below 200, 170, and 150 K for Er, Tm, and Yb compounds, respectively. At lower temperatures, the $M(H)$ curves become a straight line in a field weaker than 9 T; that is, we do not observe the MMT of the $\widetilde{SS}$ structure for RMn_6Ge_6 (R=Er-Yb) below 9 T.

Closely inspecting the $M(H)$ curves for $HoMn_6Ge_6$, we find that they behave differently from those for the other three compounds. When the magnetic structure is $\widetilde{SS}$ at 200 K, the $M(H)$ curve for $HoMn_6Ge_6$ is enhanced in magnitude, and the MMT occurs at lower field than at 300 K.

Now we try to address the nature of the MMT for $\widetilde{SS}$ and AFM structures, especially for $HoMn_6Ge_6$. The $M(H)$ isothermals for RMn_6Ge_6 have not been systematically measured in a strong magnetic field, except for $ErMn_6Ge_6$ and $DyMn_6Ge_6$ below 14 T in limited temperature ranges [50]. We performed the magnetization measurement at different temperatures for $HoMn_6Ge_6$ and $ErMn_6Ge_6$ in a pulsed magnetic field up to 57 T at the Chinese National High Magnetic Field Lab, Wuhan. Figure 9 shows the $M(H)$ isothermals for $HoMn_6Ge_6$ at some representative temperatures, and the result for $ErMn_6Ge_6$ is shown in the Supplemental Material [45]. The transition which occurs at 7 T at 300 K moves to higher field at low temperatures. This transition occurs at 22 T at 200 K and then fades out. At the same temperature, another MMT appear at 5 T at 200 K, consistent with our measurement with the MPMS. The second MMT also moves to higher field at low temperatures and remains at about 25 T below 50 K. A previous study at 4.2 K showed that the transition in the $\widetilde{SS}$ state is due to partial decoupling of the Ho-Mn interaction [38]. The external field aligns the Ho moment parallel to the c axis, while two neighboring Mn sublattices develop an AFM configuration along the c axis [see the scheme in the inset in Fig. 8(a)], which induces a large M change because large R moments are aligned.

On the other hand, the MMT in the high-temperature AFM state has the same nature as that in the RMn_6Ge_6 family. An external field forces the Mn-sublattice moments to change from the AFM arrangement to a FS structure [see the scheme in the inset in Fig. 8(c)]. This transition induces a relatively small magnetization change because the R moments are not affected.

After clarifying the MMTs for the $\widetilde{SS}$ and AFM structures, we examine the $\rho_{yx}(H)$ curves, which resemble the profile of $M(H)$ in general. In order to estimate the magnitude of

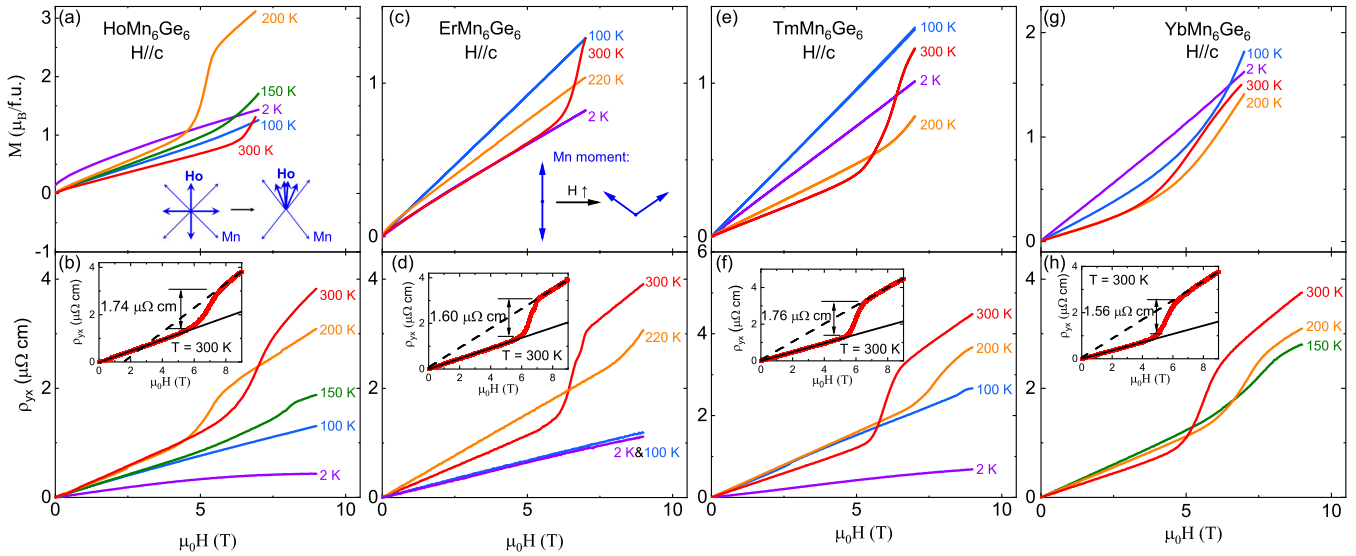

FIG. 8. Magnetization and Hall resistivity as a function of magnetic field $\mu_0 H$ for RMn$_6$Ge$_6$ (R=Ho-Yb). The schemes in the insets in (a) and (c) indicate the changes in the $\widetilde{\text{SS}}$ and AFM states when the magnetic field increases, respectively. Insets in (b), (d), (f), and (h) show the magnitude of ρ_{yx}^{A} at 300 K for RMn$_6$Ge$_6$ (R=Ho-Yb), respectively. It is noteworthy that our sample of HoMn$_6$Ge$_6$ shows a very small net spontaneous magnetization (0.15 μ_B/f.u.) at 2 K. The origin of this small net FM component is not clear, but it has no visible influence on the Hall signal.

the AHE during the MMT, we take the height of the Hall curves in the MMT as the size of anomalous Hall resistivity ρ_{yx}^{A}. As shown in the inset in Fig. 8(b), ρ_{yx}^{A} at 300 K for the Ho compound is about 1.7 μΩ cm, and the calculated anomalous Hall conductivity (AHC; $\sigma_{xy}^{A} = \rho_{yx}^{A}/\rho_{xx}^{2}$) is around 6.8 $\Omega^{-1}\,\text{cm}^{-1}$. Similarly, we calculated the AHC at 200 K for the second MMT, finding a value of 22 $\Omega^{-1}\,\text{cm}^{-1}$, which is slightly greater than that at 300 K. The obtained AHCs at 300 K for the Er, Tm, and Yb compounds have the same magnitude.

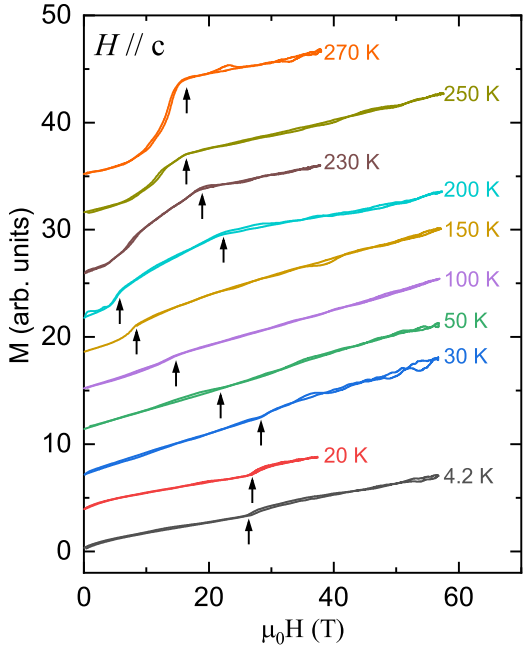

FIG. 9. Field dependence of magnetization for HoMn$_6$Ge$_6$ measured in a pulsed magnetic field up to 57 T. The arrows indicate the positions of MMT at different temperatures.

C. LuMn$_6$Ge$_6$

Because there is no 4f moment in Lu atoms, the magnetic properties of LuMn$_6$Ge$_6$ are solely determined by the Mn moments. Previous studies reported an up-up-down-down AFM ordering of the Mn moments with a Néel temperature of 527 K [35,51]. Our measurements of the temperature dependence of magnetization and resistivity demonstrate a stable magnetic structure from room temperature to 2 K (see Fig. 10). Figure 11 shows that the $M(H)$ curves have no MMT when the external field is below 7 T, yet the $\rho_{yx}(H)$ curves demonstrate a transition above 250 K at higher field. This transition is from AFM to FS, as observed for RMn$_6$Ge$_6$ (R=Ho-Yb) at room temperature [see the scheme in the inset in Fig. 11(a)] [51]. We find this transition induces a small AHC change (46 $\Omega^{-1}\,\text{cm}^{-1}$).

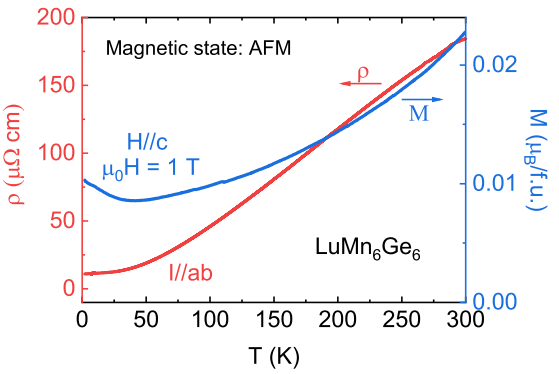

FIG. 10. Temperature dependence of resistivity and magnetization for LuMn$_6$Ge$_6$.

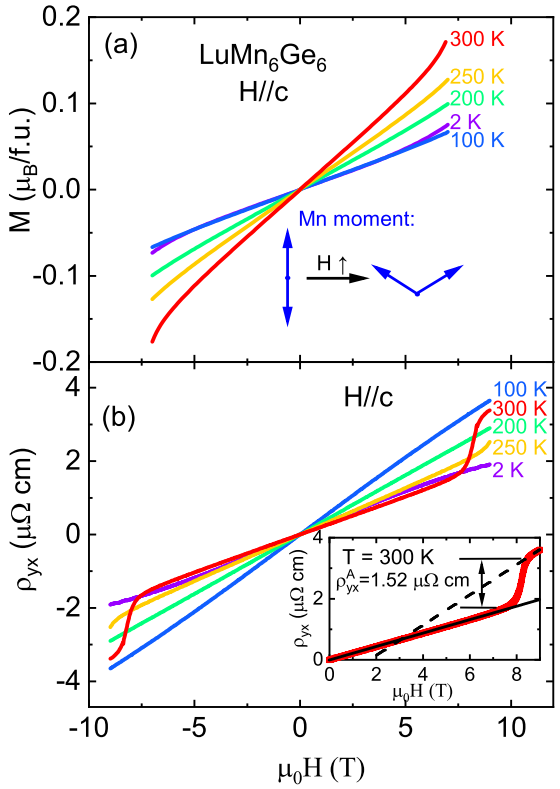

FIG. 11. Magnetization and Hall resistivity as a function of magnetic field $\mu_0 H$ for $LuMn_6Ge_6$. The inset in (b) shows the magnitude of ρ_{yx}^A at 300 K for $LuMn_6Ge_6$. The change in the Mn moment configuration in the MMT is shown in the inset in (a).

IV. DISCUSSION

We summarize the estimated AHC in the MMTs for the RMn_6Ge_6 compounds at 300 K when $H \parallel c$ in Fig. 12. The AHCs for $TbMn_6Ge_6$ when $H \perp c$ and for $HoMn_6Ge_6$ at 200 K are listed for comparison. We observe three types of MMT below 9 T, from FS to FIM of R and Mn moments, from AFM to FS of Mn moments, and from $\widetilde{SS}$ to a structure consisting of decoupled R and Mn moments. The transition from AFM to FS of Mn moments generally occurs at high temperatures in (Ho-Lu)Mn_6Ge_6, and the corresponding AHC is relatively small. We also observed a weak AHE induced by the transition of the $\widetilde{SS}$ structure in $HoMn_6Ge_6$ at 200 K. In comparison, the transition from the FS to FIM structure which contains FM ordered Mn kagomé lattices in $TbMn_6Ge_6$ and $DyMn_6Ge_6$ leads to a large AHC on the order of $\sim 10^2\ \Omega^{-1}\,\mathrm{cm}^{-1}$.

In general, the field-dependent Hall resistivity can be written as

$$\rho_{xy} = R_0 B + R_s \mu_0 M, \tag{1}$$

where R_0 and R_s are ordinary and anomalous Hall coefficients, respectively. We fit only the data for the compounds which show a pronounced MMT when $\mu_0 H < 7$ T because it is difficult to disentangle the ordinary and anomalous Hall effects when the $M(H)$ curve is close to linear. Some fitting results for Hall resistivity are shown in Fig. S3. From the results in this work, no obvious topological Hall effect is observed. Table I shows that the values of R_s are much larger than R_0 at high temperature. Taking into account the change in the $M(H)$ curve in the MMT, we calculated the values of AHC change in the MMT σ_{xy}^A from R_s, and the results are the same as we estimated directly for the $\rho_{yx}(H)$ curves. We notice that the R_s value for $TbMn_6Ge_6$ for $H \parallel c$ is larger than that for other compounds, which is consistent with the observation that the transition from the FS to FIM structure leads to a large AHC.

The fitting of the Hall resistivity at the base temperature gives a reasonable estimation of the carrier type and density because the ordinary Hall effect (OHE) is dominant. In general the compounds show a p-type OHE, and the hole density is estimated to be about $1 \times 10^{22}\,\mathrm{cm}^{-3}$. The results can be found in the Supplemental Material [45]. It is noteworthy that $TbMn_6Ge_6$ shows an OHE slightly different from that of other compounds. R_0 of $TbMn_6Ge_6$ at 2 K is the largest among all compounds for $H \parallel c$, corresponding to a low carrier density of $2.7 \times 10^{21}\,\mathrm{cm}^{-3}$. When $H \parallel ab$ plane, the R_0 value is negative. There seems to be an anisotropic carrier type under different field directions in $TbMn_6Ge_6$, similar to that in YMn_6Sn_6 [21]. It may reflect an electronic structure change when the magnetization is along different crystallographic orientations. Further band calculations will be helpful for figuring out the anisotropic carrier type in $TbMn_6Ge_6$.

We now focus on the AHE in $TbMn_6Ge_6$. In general, the anomalous Hall resistivity has the following relation to the resistivity: $\rho_{yx}^A = \alpha \rho_{xx} + \beta \rho_{xx}^2$, in which the first term

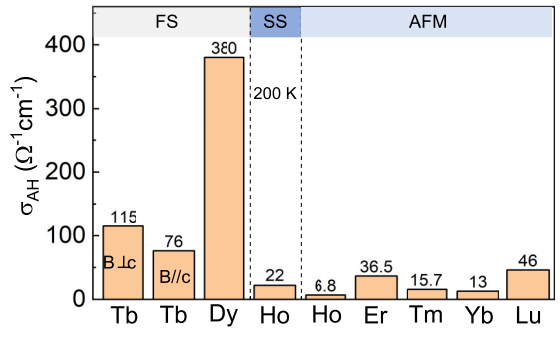

FIG. 12. Magnitude of AHC for different RMn_6Ge_6 compounds at 300 K when $H \parallel c$ axis. The AHCs for $TbMn_6Ge_6$ when $H \perp c$ axis and for $HoMn_6Ge_6$ at 200 K are listed for comparison.

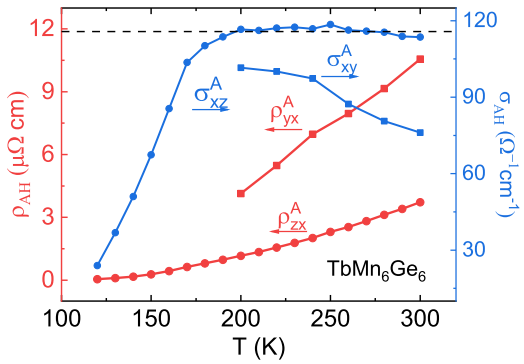

FIG. 13. Temperature dependence of anomalous Hall resistivities and conductivities in the xy and xz planes for $TbMn_6Ge_6$.

TABLE I. Fitting results of the AHE for selected RMn$_6$Ge$_6$ compounds. σ'_{AH} represents the AHC change in the MMT obtained by fitting the field-dependent Hall resistivity, while σ_{AH} is the AHC change in the MMT that we estimate directly in the ρ_{yx} curves. The value of R_0 for TbMn$_6$Ge$_6$ in $H \parallel c$ is not shown because it is too small to determine its sign. The fitting details for the Hall resistivity can be found in the Supplemental Material [45].

R	Configuration	R_0 ($\mu\Omega$ cm/T)	R_s ($\mu\Omega$ cm/T)	M (μ_B/f.u.)	σ'_{AH} (Ω^{-1} cm^{-1})	σ_{AH} (Ω^{-1} cm^{-1})
Tb	$\parallel c$, 300 K		34.9	5.4	80	76
Tb	$\parallel ab$, 300 K	−0.03	11.8	5.2	113	115
Dy	$\parallel c$, 200 K	0.12	12.3	1.1	117	128
Ho	$\parallel c$, 200 K	0.11	8.3	1.7	19	22

represents the extrinsic skew-scattering contribution, while the second term represents an intrinsic plus side-jump contribution [52]. When the resistivity changes little in magnetic field, the anomalous Hall conductivity can then be written as $\sigma^A_{yx} = \alpha/\rho_{xx} + \beta$. Because ρ_{xx} of RMn$_6Ge_6$ changes largely with temperature, a purely intrinsic AHC should be invariant with respect to the temperature.

Figure 13 shows the temperature dependence of anomalous Hall resistivities and conductivities for TbMn$_6$Ge$_6$ when $H \parallel c$ and $H \perp c$. When the external field is along the c axis, σ^A_{xy} clusters in the range between 75 and 100 Ω^{-1} cm^{-1} from 300 to 200 K. This value is close to that for TbMn$_6$Sn$_6$ (120 Ω^{-1} cm^{-1} [12]), which indicates its intrinsic origin. On the other hand, the temperature dependence of the AHC for $H \perp c$ is different. It shows a plateau around 115 Ω^{-1} cm^{-1} above 200 K and then significantly drops below this temperature. This unusual behavior is unlike any observation for the RMn$_6$Sn$_6$ compounds [16,53]. An intrinsic contribution which dominates at high temperature plus an opposite extrinsic one can produce this particular temperature dependence. Further study of the electronic and magnetic structure will help us to deeply understand the AHE in TbMn$_6$Ge$_6$.

V. CONCLUSION

In summary, we studied the AHE for single crystals of RMn$_6$Ge$_6$ (R=Tb-Lu), a group of Mn-based kagomé magnets. The RMn$_6$Ge$_6$ compounds exhibit complicated magnetic structures in zero field and different types of MMTs in an external magnetic field, concomitant with AHE. We identified three kinds of AHEs corresponding to different magnetic structure changes.

(1) The AFM alignment of Mn moments in RMn$_6$Ge$_6$ (R=Ho-Lu) at high temperatures deform in an external field along the c axis and form an FS structure. This transition leads to a relatively weak AHE.

(2) The R moments in the $\widetilde{\text{SS}}$ structure decouple from the Mn moments in an external field, leading to a structure consisting of aligned R moments and AFM Mn moments. This transition also induces a weak AHE.

(3) The FS structure of TbMn$_6$Ge$_6$ and DyMn$_6$Ge$_6$ changes to the FIM state consisting of antiparallel FM ordered R and Mn lattices in a magnetic field, which produces a considerable AHE.

By comparing the different sources of AHE, we conclude that the change in Mn moments produces a stronger AHE than that of the change in R moments. The AHEs in TbMn$_6$Ge$_6$ generally have an intrinsic origin when the external field drives the magnetic structure to the FIM state along the c axis. No clear hint of nontrivial topology is found in other compounds. Our study determined the AHE associated with different MMTs in the family of RMn$_6$Ge$_6$. Considering the wealth of magnetic structures in RMn$_6$Ge$_6$, we believe that the family can be a potential platform for studying the relationship between novel quantum phases and spin textures in kagomé lattices.

ACKNOWLEDGMENTS

The authors thank Y. Li for assistance in modifying the figures. S.J. was supported by the National Natural Science Foundation of China (Grant No. U1832214), the Interdisciplinary Program of Wuhan National High Magnetic Field Center (Grant No. WHMFC202123), Huazhong University of Science and Technology, the National Key R&D Program of China (Grant No. 2018YFA0305601), and the strategic Priority Research Program of the Chinese Academy of Sciences (Grant No. XDB28000000). J.W. was supported by the National Natural Science Foundation of China (Grant No. 12074135). H.Z. acknowledges support from the China Postdoctoral Science Foundation (Grant No. 2021M701971) and the Guangdong Basic and Applied Basic Research Foundation (Grant No. 2022A1515110322).

[1] E. Liu *et al.*, Nat. Phys. **14**, 1125 (2018).
[2] L. Ye, M. Kang, J. Liu, F. von Cube, C. R. Wicker, T. Suzuki, C. Jozwiak, A. Bostwick, E. Rotenberg, D. C. Bell, L. Fu, R. Comin, and J. G. Checkelsky, Nature (London) **555**, 638 (2018).
[3] M. Kang *et al.*, Nat. Mater. **19**, 163 (2020).
[4] S. Nakatsuji, N. Kiyohara, and T. Higo, Nature (London) **527**, 212 (2015).
[5] J.-X. Yin, S. S. Zhang, G. Chang, Q. Wang, S. S. Tsirkin, Z. Guguchia, B. Lian, H. Zhou, K. Jiang, I. Belopolski, N. Shumiya, D. Multer, M. Litskevich, T. A. Cochran, H. Lin, Z. Wang, T. Neupert, S. Jia, H. Lei, and M. Z. Hasan, Nat. Phys. **15**, 443 (2019).
[6] J.-X. Yin, S. S. Zhang, H. Li, K. Jiang, G. Chang, B. Zhang, B. Lian, C. Xiang, I. Belopolski, H. Zheng, T. A. Cochran, S.-Y. Xu, G. Bian, K. Liu, T.-R. Chang, H. Lin, Z.-Y. Lu, Z. Wang,

S. Jia, W. Wang, and M. Z. Hasan, Nature (London) **562**, 91 (2018).
[7] H. Zhou, G. Chang, G. Wang, X. Gui, X. Xu, J.-X. Yin, Z. Guguchia, S. S. Zhang, T.-R. Chang, H. Lin, W. Xie, M. Z. Hasan, and S. Jia, Phys. Rev. B **101**, 125121 (2020).
[8] Z. Lin, J.-H. Choi, Q. Zhang, W. Qin, S. Yi, P. Wang, L. Li, Y. Wang, H. Zhang, Z. Sun, L. Wei, S. Zhang, T. Guo, Q. Lu, J.-H. Cho, C. Zeng, and Z. Zhang, Phys. Rev. Lett. **121**, 096401 (2018).
[9] G. Xu, B. Lian, and S.-C. Zhang, Phys. Rev. Lett. **115**, 186802 (2015).
[10] F. D. M. Haldane, Phys. Rev. Lett. **61**, 2015 (1988).
[11] E. Tang, J.-W. Mei, and X.-G. Wen, Phys. Rev. Lett. **106**, 236802 (2011).
[12] J.-X. Yin *et al.*, Nature (London) **583**, 533 (2020).
[13] X. Xu, J.-X. Yin, W. Ma, H.-J. Tien, X.-B. Qiang, P. V. S. Reddy, H. Zhou, J. Shen, H.-Z. Lu, T.-R. Chang, Z. Qu, and S. Jia, Nat. Commun. **13**, 1197 (2022).
[14] H. Zhang, J. Koo, C. Xu, M. Sretenovic, B. Yan, and X. Ke, Nat. Commun. **13**, 1091 (2022).
[15] W. Ma, X. Xu, J.-X. Yin, H. Yang, H. Zhou, Z.-J. Cheng, Y. Huang, Z. Qu, F. Wang, M. Z. Hasan, and S. Jia, Phys. Rev. Lett. **126**, 246602 (2021).
[16] W. Ma, X. Xu, Z. Wang, H. Zhou, M. Marshall, Z. Qu, W. Xie, and S. Jia, Phys. Rev. B **103**, 235109 (2021).
[17] L. Gao, S. Shen, Q. Wang, W. Shi, Y. Zhao, C. Li, W. Cao, C. Pei, J.-Y. Ge, G. Li, J. Li, Y. Chen, S. Yan, and Y. Qi, Appl. Phys. Lett. **119**, 092405 (2021).
[18] Y. Lee, R. Skomski, X. Wang, P. P. Orth, A. K. Pathak, B. N. Harmon, R. J. McQueeney, I. I. Mazin, and L. Ke, arXiv:2201.11265.
[19] C. Mielke III *et al.*, Commun. Phys. **5**, 107 (2022).
[20] N. J. Ghimire, R. L. Dally, L. Poudel, D. C. Jones, D. Michel, N. T. Magar, M. Bleuel, M. A. McGuire, J. S. Jiang, J. F. Mitchell, J. W. Lynn, and I. I. Mazin, Sci. Adv. **6**, eabe2680 (2020).
[21] Q. Wang, K. J. Neubauer, C. Duan, Q. Yin, S. Fujitsu, H. Hosono, F. Ye, R. Zhang, S. Chi, K. Krycka, H. Lei, and P. Dai, Phys. Rev. B **103**, 014416 (2021).
[22] K. Uhlířová, F. de Boer, and V. Sechovský, in *WDS'06 Proceedings of Contributed Papers* (MatfyzPress, Prague, 2006), Vol. 3, p. 48.
[23] B. Malaman, G. Venturini, B. Chafik El Idrissi, and E. Ressouche, J. Alloys Compd. **252**, 41 (1997).
[24] B. Malaman, G. Venturini, R. Welter, J. Sanchez, P. Vulliet, and E. Ressouche, J. Magn. Magn. Mater. **202**, 519 (1999).
[25] D. Clatterbuck and K. Gschneidner, J. Magn. Magn. Mater. **207**, 78 (1999).
[26] M. Li, Q. Wang, G. Wang, Z. Yuan, W. Song, R. Lou, Z. Liu, Y. Huang, Z. Liu, H. Lei, Z. Yin, and S. Wang, Nat. Commun. **12**, 3129 (2021).
[27] A. Kitaori, N. Kanazawa, T. Yokouchi, F. Kagawa, N. Nagaosa, and Y. Tokura, Proc. Natl. Acad. Sci. U.S.A. **118**, e2105422118 (2021).
[28] D. Chen, C. Le, C. Fu, H. Lin, W. Schnelle, Y. Sun, and C. Felser, Phys. Rev. B **103**, 144410 (2021).
[29] G. Venturini, B. Chafik El Idrissi, E. Ressouche, and B. Malaman, J. Alloys Compd. **216**, 243 (1995).
[30] P. Schobinger-Papamantellos, F. Altorfer, J. Brabers, F. de Boer, and K. Buschow, J. Alloys Compd. **203**, 243 (1994).
[31] P. Schobinger-Papamantellos, J. Brabers, and K. Buschow, J. Magn. Magn. Mater. **139**, 119 (1995).
[32] P. Schobinger-Papamantellos, G. André, J. Rodríguez-Carvajal, and K. Buschow, J. Alloys Compd. **219**, 176 (1995).
[33] P. Schobinger-Papamantellos, G. André, J. Rodríguez-Carvajal, J. Brabers, and K. Buschow, J. Alloys Compd. **226**, 113 (1995).
[34] T. Mazet, H. Ihou-Mouko, D. H. Ryan, C. J. Voyer, J. M. Cadogan, and B. Malaman, J. Phys.: Condens. Mat. **22**, 116005 (2010).
[35] P. Schobinger-Papamantellos, G. André, J. Rodríguez-Carvajal, J. Brabers, and K. Buschow, J. Alloys Compd. **226**, 152 (1995).
[36] J. Brabers, V. Duijn, F. de Boer, and K. Buschow, J. Alloys Compd. **198**, 127 (1993).
[37] L. Zhang, J. C. P. Klaasse, E. Brück, K. H. J. Buschow, F. R. de Boer, S. Yoshii, K. Kindo, C. Lefèvre, and G. Venturini, Phys. Rev. B **70**, 224425 (2004).
[38] L. Zhang, Ph.D. thesis, Universiteit van Amsterdam, 2005.
[39] T. Mazet, R. Welter, G. Venturini, E. Ressouche, and B. Malaman, Solid State Commun. **110**, 407 (1999).
[40] G. Venturini, R. Welter, B. Malaman, and E. Ressouche, J. Alloys Compd. **200**, 51 (1993).
[41] H. Ihou-Mouko, T. Mazet, O. Isnard, and B. Malaman, J. Alloys Compd. **426**, 26 (2006).
[42] M. Brooks, L. Nordström, and B. Johansson, Physica B (Amsterdam, Neth.) **172**, 95 (1991).
[43] P. Schobinger-Papamantellos, J. Schefer, J. Brabers, and K. Buschow, J. Alloys Compd. **215**, 111 (1994).
[44] H. Duijn, E. Brück, K. Buschow, and F. de Boer, J. Magn. Magn. Mater. **196–197**, 691 (1999).
[45] See Supplemental Material at http://link.aps.org/supplemental/10.1103/PhysRevMaterials.7.024404 for the details of the crystal growth and structural characterizations as well as additional figures and discussion, which includes Refs. [54,55].
[46] R. D. Shannon and C. T. Prewitt, Acta Crystallogr., Sect. B **26**, 1046 (1970).
[47] S. Yoshii, K. Kindo, L. Zhang, E. Brück, K. Buschow, F. de Boer, C. Lefèvre, and G. Venturini, J. Alloys Compd. **408–412**, 173 (2006).
[48] P. Schobinger-Papamantellos, J. Rodríguez-Carvajal, G. André, and K. Buschow, J. Magn. Magn. Mater. **150**, 311 (1995).
[49] A. Mar, C. Lefèvre, and G. Venturini, J. Magn. Magn. Mater. **269**, 380 (2004).
[50] K. Uhlírová, V. Sechovský, F. R. de Boer, S. Yoshii, K. Nishikawa, M. Hagiwara, K. Kindo, and G. Venturini, J. Phys.: Conf. Ser. **51**, 123 (2006).
[51] M. Koyama, Y. Narumi, S. Yoshii, K. Kindo, L. Zhang, E. Brück, K. Buschow, F. de Boer, C. Lefèvre, and G. Venturini, J. Alloys Compd. **408–412**, 161 (2006).
[52] C. Zeng, Y. Yao, Q. Niu, and H. H. Weitering, Phys. Rev. Lett. **96**, 037204 (2006).
[53] T. Asaba, S. M. Thomas, M. Curtis, J. D. Thompson, E. D. Bauer, and F. Ronning, Phys. Rev. B **101**, 174415 (2020).
[54] M. A. Avila, T. Takabatake, Y. Takahashi, S. L. Bud'ko, and P. C. Canfield, J. Phys.: Condens. Mat. **17**, 6969 (2005).
[55] P. C. Canfield, T. Kong, U. S. Kaluarachchi, and N. H. Jo, Philos. Mag. **96**, 84 (2016).